Simultaneous electromagnetically induced transparency for two circularly polarized lasers coupled to the same linearly polarized laser in a four-level atomic system in the W scheme

Cristian Bahrim[*] and Chris Nelson[†]
Department of Physics, Lamar University, P.O. Box 10046, Beaumont, Texas 77710, USA
(Received 15 July 2010; published 7 March 2011)

Electromagnetic induced transparency (EIT) can be produced in a four-level atomic system in the W scheme using a linearly polarized optical field for simultaneously slowing down two σ^+ and σ^- circularly polarized optical fields. This four-level atomic system can be set up with a $|^1S_0\rangle$ ground state and three Zeeman levels of the $|^1P_1\rangle$ excited state of any alkali-metal atom placed in a weak magnetic field. We apply our W scheme to ultracold magnesium atoms for neglecting the collisional dephasing. Atomic coherences are reported after solving a density matrix master equation including radiative relaxations from Zeeman states of the $|^1P_1\rangle$ multiplet to the $|^1S_0\rangle$ ground state. The EIT feature is analyzed using the transit time between the normal dispersive region and the EIT region. The evolution of the EIT feature with the variation of the coupling field is discussed using an intuitive dressed-state representation. We analyze the sensitivity of an EIT feature to pressure broadening of the excited Zeeman states.

DOI: 10.1103/PhysRevA.83.033804 PACS number(s): 42.50.Gy

I. INTRODUCTION

Electromagnetic induced transparency (EIT) is a quantum interference phenomenon which occurs in optically thick media where the atoms are prepared in a coherent superposition of states as the result of the interaction between optical fields and atomic states. In EIT, quantum interference eliminates the absorption of a propagating weak probe field in resonance to an atomic transition due to a strong coupling field resonant to another linked transition. Since the pioneering work done by Harris *et al.* [1], extensive efforts were dedicated both in theory and in experiment for enlarging the panel of possible applications of the EIT phenomenon, including slow and stopped light [2–4], lasing without inversion [5], Kerr nonlinearity associated with cross-phase modulation [6] or spatially modulated transparency [7], quantum entanglement [8], etc. The review article by Fleischhauer *et al.* [9] summarizes the achievements generated by the EIT technique in the field of nonlinear optics and quantum information and also discusses possible new applications.

In recent years, many extensive studies have been devoted to three-level atomic systems, such as the V system [8,10], the Λ system [11], and the ladder system [12], in which two optical fields are used and, due to quantum interference, one of them is slowed down. Recently, the propagation of a weak probe field in various laser-driven four-level atomic systems was investigated [13]. Also, a double EIT structure with controlled group velocity was observed in the interaction between three laser beams with a four-level atom in a tripod configuration [14]. The tripod is formed by three lower atomic states and one upper state interacting simultaneously with three optical fields incident on the lower states for slowing down one weak probe field using the other two lasers as coupling fields. Two group velocities for the probe field were generated when different detunings for each coupling field were used in the calculations from [14]. However, when the detuning of the two coupling fields was considered the same, they observed a single transparency window and generated a single group velocity for the weak probe field, thus reducing their tripod system to one Λ system.

Even a five-level atom (M-type) system interacting with two pairs of near-resonant laser fields was recently proposed [15]. Experimental efforts were devoted in using a four-level system with a triplet ground state and an excited state interacting with two lasers and one radio-frequency field resonant to the transition between one hyperfine level of the ground state and one of the other two hyperfine levels in a Λ-type system [16]. A similar tripod system was theoretically predicted by using two circularly polarized fields driven by a linearly polarized field [17]. However, the hypothesis of simultaneously creating two EITs in a four-level atomic system in the W scheme (or a reverse tripod) has, to the best of our knowledge, never been explored. We consider this W system to be important for new applications in quantum information processing, including binary recording using angular momenta $+\hbar$ and $-\hbar$ of the photons in two σ^+ and σ^- circularly polarized laser beams.

This article will show that a W scheme can be set up so that it satisfies the necessary conditions [9] for the simultaneous creation of two stable EIT features. Our W scheme is formed by a four-level atomic system interacting with two σ^+ and σ^- circularly polarized optical fields which are simultaneously slowed down by a common linearly polarized coupling field. Solving the density matrix master equation for the coupling between these optical fields and the atomic system provides both statistical and quantum mechanical information [18]. This method is appropriate to be used whenever the wavelength of the optical field is large enough to enshroud a large number of atoms.

The article is structured as follows: Section II presents a four-level atomic system in the W scheme using magnesium atoms placed in a weak magnetic field. Section III gives details regarding our quantum model based on the density matrix

[*]cristian.bahrim@lamar.edu
[†]Present address: Department of Natural and Environmental Sciences, Western State College, Gunnison, Colorado 81230, USA.

formalism and applied to a bulk of gaseous ultra-cold atoms. Section IV reports results for atomic coherences, discusses the criteria for the formation of two stable EITs, describes the characteristics of the EIT features such as the slope and the width of the atomic coherences, and shows their variation with the strength of the B field and the pressure broadening of the atomic levels. The analysis of the atomic coherences as a function of the coupling field, in a W scheme, using an intuitive dressed-state representation, is given in Sec. V. Our conclusion follows in Sec. VI.

II. A FOUR-LEVEL W SYSTEM

Figure 1 shows an energy diagram of a four-level atomic system in a W scheme. The four-level atom represents an alkali-metal atom placed in a weak magnetic field, which produces a normal Zeeman splitting of a three-fold degenerate $|^1P_1\rangle$ first excited state into three levels, labeled $|^1P_1; M=-1\rangle = |1\rangle$,$|^1P_1; M=0\rangle = |2\rangle$, and $|^1P_1; M=+1\rangle = |3\rangle$. The fourth level is the $|^1S_0\rangle$ ground state and it will be labeled by $|0\rangle$. The strength of the B field should be weak enough to make the interaction $(-\vec{\mu}\cdot\vec{B})$ with the net atomic magnetic moment $\vec{\mu}$ smaller than the spin-orbit $\vec{L}\cdot\vec{S}$ coupling in the atomic Hamiltonian [19]. In such a case, the operators $\mathbf{L}^2$, $\mathbf{S}^2$, and $\mathbf{J}^2$ (where $\mathbf{J}=\mathbf{L}+\mathbf{S}$) give good quantum numbers for atomic states placed in a weak B field.

Figure 1 shows the resonant atomic frequencies for the three dipole-allowed transitions from the $|^1S_0\rangle$ state to the $|^1P_1\rangle$ multiplet: ω_{01} for $|0\rangle \to |1\rangle$, ω_{02} for $|0\rangle \to |2\rangle$, and ω_{03} for $|0\rangle \to |3\rangle$. The states $|1\rangle$ and $|3\rangle$ are separated from $|2\rangle$ by the Larmor frequency

$$\bar{\omega} = \frac{g\mu_B B}{\hbar}, \tag{1}$$

where $\mu_B = 9.27408\times10^{-24}$ J/T is the Bohr magneton and g is the Landé factor, which equals 1 for a $|^1P_1\rangle$ state placed in a weak B field [19], and $\hbar$ is Planck's constant divided by 2π. Thus, the atomic frequencies are

$$\omega_{01} = \omega_0 - \varpi, \quad \omega_{02} = \omega_0, \quad \omega_{03} = \omega_0 + \varpi. \tag{2}$$

The frequencies of the E field are detuned from the atomic frequencies ω_{0j} by Δ_j as follows:

$$\omega_j = \Delta_j + \omega_{0j}, \tag{3}$$

where ω_1 (for $j=1$) is the frequency of a σ^- circularly $(-\hbar)$ polarized field for transition $|0\rangle \to |1\rangle$, ω_2 (for $j=2$) is the frequency of a linearly polarized field for transition $|0\rangle \to |2\rangle$, and ω_3 (for $j=3$) is the frequency of a σ^+ circularly $(+\hbar)$ polarized field for transition $|0\rangle \to |3\rangle$.

In this article we investigate the possibility of simultaneously generating two stable EITs in a four-level atomic system in a W scheme, which is in a steady state completely determined by two static parameters: the detuned laser frequencies ω_j given by Eq. (3) and the intensities I_j of three laser beams (see Fig. 1). For that, a time-independent atom-field Hamiltonian

$$H = H_0 + H_I \tag{4}$$

is used. In Eq. (4) the zero-order Hamiltonian is

$$H_0 = \hbar\omega_{00}|0\rangle\langle 0| + \sum_{j=1}^{3}\hbar\omega_{0j}|j\rangle\langle j|, \tag{5}$$

to which an interaction Hamiltonian

$$H_I = -\frac{\hbar}{2}\sum_{j=1}^{3}\Omega_j e^{i\phi_j}e^{i\Delta_j t}|0\rangle\langle j| \tag{6}$$

is added. We work within a rotating-wave approximation which keeps only the energy-conserving terms [18]. In (6), the terms $\Omega_1 e^{i\varphi_1}$, $\Omega_2 e^{i\varphi_2}$, and $\Omega_3 e^{i\varphi_3}$ represent complex static Rabi frequencies associated to the interaction between E fields resonant with the three atomic transitions shown in Fig. 1 and the respective atomic dipole moments. According to Fleischhauer *et al.* [9], in the rotating-wave approximation we can represent the interaction Hamiltonian given in (6) with real-valued Rabi frequencies in a rotating frame. This corresponds to neglecting propagation effects, as it will be discussed in Section III, in relation to the master equation. The Rabi frequency

$$\Omega_j = \frac{\mu_j E_j}{\hbar} \tag{7}$$

represents the energy associated with the E-field–atomic-dipole interaction, where E_j is the amplitude of the optical field, $E_j = \sqrt{2c\mu_0 I_j}$ (where I_j is the intensity of the optical field, c is the speed of the light in free space, and μ_0 is the permeability of free space), and $\mu_j = \sqrt{3\hbar c^3\Gamma_j/(4\omega_j^3)}$ is the dipole moment for each atomic state $|j\rangle$ (where $j=1$, 2, or 3 and Γ_j is the natural width of a Zeeman state $|j\rangle$).

The time-dependent Schrödinger equation, including the time-independent Hamiltonian (4), has as a solution a

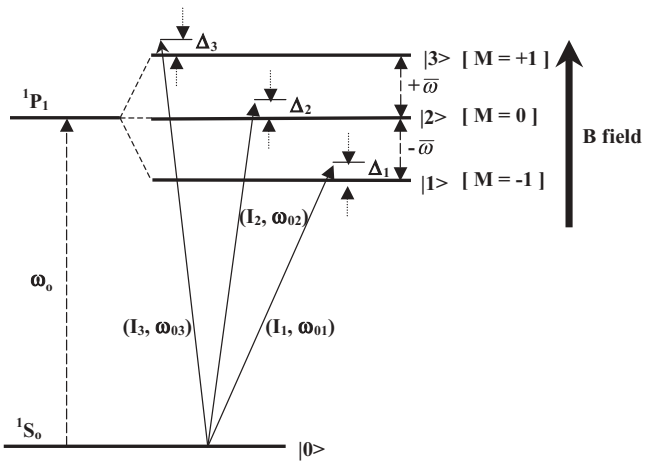

FIG. 1. Our four-level atomic system in a W scheme. Each transition $|0\rangle \to |j\rangle$ is characterized by the intensity of the optical field, I_j and the resonant frequency, ω_{oj} (where $j=1$, 2, or 3). Δ_j is the detuning of an E field resonant to a Zeeman state $|j\rangle$.

time-dependent interaction wave function:

$$|\Psi(t)\rangle = C_0(t)e^{-i\omega_{00}t}|0\rangle + \sum_{j=1}^{3} C_j(t)\, e^{-i(\omega_{0j}-\Delta_j)t}|j\rangle, \quad (8)$$

where the temporal part of $|\Psi(t)\rangle$ is independent of the time-independent counterpart $\{|0\rangle, |j\rangle\}$.

The four-level atom is created by choosing a B field so that there is no overlapping between the widths of the Zeeman levels. This criterion limits the range of the B field, as shown below. If we consider Γ_0 as being the rate of spontaneous emission from the $|^1P_1\rangle$ state to the $|^1S_0\rangle$ state, then the decay rates of the $|^1P_1; M = +1\rangle$ and $|^1P_1; M = -1\rangle$ states are

$$\Gamma_1 = \Gamma_0\left(\frac{\omega_0 - \bar{\omega}}{\omega_0}\right)^3 \quad \text{and} \quad \Gamma_3 = \Gamma_0\left(\frac{\omega_0 + \bar{\omega}}{\omega_0}\right)^3. \quad (9)$$

The decay rate of the state $|^1P_1; M = 0\rangle$ is labeled as $\Gamma_2 = \Gamma_0$. Equations (9) can readily be proven using the formulas for radiative decay rates Γ_j given in Sec. 9.2 of [20], which shows that Γ_j is proportional to $4\omega_j^3/(9\hbar c^3)$, where ω_j is the angular frequency for any of the transitions $|^1P_1; M = 0, \pm 1\rangle \rightarrow |^1S_0\rangle$. The decay rate to the $|^1S_0\rangle$ state from the $|^1P_1; M = +1\rangle$ state is $\Gamma_3 = 4C(\omega_0 + \bar{\omega})^3/(9\hbar c^3)$, from $|^1P_1; M = -1\rangle$ it is $\Gamma_1 = 4C(\omega_0 - \bar{\omega})^3/(9\hbar c^3)$, and from $|^1P_1; M = 0\rangle$ it is $\Gamma_2 = 4C\omega_0^3/(9\hbar c^3)$, where C is a common constant. A simple mathematical manipulation leads to formulas (9).

In our theoretical model, we choose magnesium atoms, for which the transition from the $|^1P_1\rangle$ state to the $|^1S_0\rangle$ state has a vacuum wavelength λ_0 of 285.28 nm and an associated angular frequency ω_0 of 6.605×10^{15} Hz [20]. The B field should be weak enough so that the Larmor frequency from Eq. (1) is much smaller than the characteristic time of the spin-orbit interaction:

$$\bar{\omega} \ll \frac{1}{\tau_{S-0}}. \quad (10)$$

For the magnesium atom, the radiative decay between the $|^1S_0\rangle$ and $|^1P_1\rangle$ states is 79 MHz [20]. Because τ_{S-0} is 2.02 ns in our case, the boundary condition (10) is verified for $B < 0.035$ T.

Also, the B field should be strong enough to remove the degeneracy of the $|^1P_1\rangle$ state, and to resolve the $|^1P_1; M\rangle$ sublevels so that no overlapping exists between the absorption band widths of the Zeeman states. This second boundary condition can be written as:

$$\bar{\omega} \gg \frac{\Gamma_1 + \Gamma_2}{2} \quad \text{and} \quad \bar{\omega} \gg \frac{\Gamma_2 + \Gamma_3}{2}. \quad (11)$$

Applying the condition (11) to $\mathrm{Mg}(^1P_1)$ atoms leads to a value of the B field larger than 0.0058 T. Therefore, the range of B fields in our calculations should be between 0.0058 and 0.035 T.

III. THEORETICAL MODEL

The linear response of an atomic system to a resonant optical field is described by the first-order complex susceptibility χ. The imaginary part of the susceptibility, $\mathrm{Im}[\chi]$ determines the absorption of an optical field in an atomic system, while the real part $\mathrm{Re}[\chi]$ determines its dispersion [9]. The $\mathrm{Re}[\chi]$ follows the usual dispersion profile when a resonant optical field is absorbed by an atomic transition, showing an anomalous dispersion, with a steep decrease of the $\mathrm{Re}[\chi]$ as a function of the field's frequency in the central part of the absorption line of width Γ. In the presence of a second (coupling) field, stronger than the first (probe) field, the atomic system becomes transparent to the resonant probe field, because the resonant transition is locked by the coupling field. Now, EIT is produced with a large enhancement of the nonlinear susceptibility in the spectral region of the induced transparency of an atomic system, which leads to a steeper increase of $\mathrm{Re}[\chi]$ within the band width. The evolution of the atomic system in the optical fields can be well described using the density matrix formalism. The phase information associated with the evolution of the atomic states $|j\rangle$ is contained in "atomic coherences" ρ_{0j}, which are solutions of the density matrix master equation. For example, the transitions $|0\rangle \rightarrow |1\rangle$ and $|0\rangle \rightarrow |3\rangle$ have linear susceptibilities depending on ρ_{01} and ρ_{03} [21] as follows:

$$\chi_1 = \frac{2N\mu_1^2}{\hbar\Omega_1}\rho_{01} \quad \text{and} \quad \chi_3 = \frac{2N\mu_3^2}{\hbar\Omega_3}\rho_{03}, \quad (12)$$

where N represents the atomic density. In our model, we will consider an ultracold atomic gas, so that we can neglect the collisional dephasing among the Zeeman states and the Doppler broadening. The atomic density for an ultracold atomic system is typically about 6×10^{17} atoms/m^3 [3].

The density matrix master equation

$$\dot{\rho} = -\frac{i}{\hbar}[H, \rho] - \frac{1}{2}(\gamma\rho + \rho\gamma) \quad (13)$$

is used for a statistical as well as quantum mechanical description of the interaction between optical fields with large wavelengths and large ensembles of atoms. In this case, a vacuum wavelength of 285.29 nm for the transition $|^1S_0\rangle \rightarrow |^1P_1\rangle$ enshrouds indeed a very large number of Mg atoms. In Eq. (13), γ represents the relaxation matrix and H is the total atom-field Hamiltonian from Eq. (4). For any ijth density matrix element, Eq. (13) is written as

$$\dot{\rho}_{ij} = -\frac{i}{\hbar}\sum_k (H_{ik}\rho_{kj} - \rho_{ik}H_{kj}) - \frac{1}{2}\sum_k (\gamma_{ik}\rho_{kj} + \rho_{ik}\gamma_{kj}). \quad (14)$$

In the present calculations done for an ultracold magnesium atomic system, we include only the radiative dephasing rates $\gamma_{ij} = \frac{1}{2}(\Gamma_i + \Gamma_j)$ as the result of spontaneous emissions:

$$\gamma_{12} = \tfrac{1}{2}(\Gamma_1 + \Gamma_2), \quad \gamma_{13} = \tfrac{1}{2}(\Gamma_1 + \Gamma_3), \quad \gamma_{14} = \tfrac{1}{2}(\Gamma_1 + \Gamma_4),$$
$$\gamma_{23} = \tfrac{1}{2}(\Gamma_2 + \Gamma_3), \quad \gamma_{34} = \tfrac{1}{2}(\Gamma_3 + \Gamma_4), \quad \gamma_{24} = \tfrac{1}{2}(\Gamma_2 + \Gamma_4). \quad (15)$$

We are solving Eq. (14) using the most favorable initial conditions for establishing EIT:

$$\rho_{00} = 1, \quad \rho_{11} = \rho_{22} = \rho_{33} = 0, \quad (16)$$

which in our case effectively traps the population of the atomic system on the $|^1S_0\rangle$ ground state [22]. The condition (16) is better fulfilled when the probe field is weaker than the coupling field [14]. For closeness, we impose that $\sum_{j=0}^{3}\rho_{jj} = 1$.

According to Fleischhauer *et al.* [9], as long as the propagation effects are not considered, which corresponds to a steady-state solution of the master equation (14), we can assume real-valued Rabi frequencies in the interaction Hamiltonian given in (6). Indeed, if the Rabi frequencies are real initially, they should remain real throughout the interaction process when the propagation effects are neglected. Therefore, we will neglect the complex phases ϕ_j in (6). This approach simplifies considerably the calculation of the master equation (14), and it has been adopted in several other publications, including [23] for a three-level Λ-type system.

A model with lesser restrictive initial conditions than given in (16) and including the collisional dephasing in our density master equation will be subject to future studies. In this article, we shall limit ourselves to showing the influence of the pressure broadening of the Zeeman states on the characteristics of the EIT feature (see Section IV H).

Similar to the three-level models from [18], the total Hamiltonian from (4) can be written as

$$H = -\left[\sum_{j=1}^{3}\left(\frac{\hbar\Omega_j}{2}|0\rangle\langle j| + \hbar\Delta_j|j\rangle\langle j|\right)\right] + \sum_{\substack{i,\,k=1\\(i\neq k)}}^{3} H_{ik}. \tag{17}$$

When the collisional dephasing is neglected in (17), the intramultiplet transitions are neglected and the off-diagonal terms H_{12}, H_{13} and H_{23} (as well as their symmetric counterparts) can be eliminated. However, these off-diagonal terms could have contributions from the radiative decay. But because of Laporte's rule, which requires the parity of the atomic states to change during a radiative transition, the dipole matrix elements between the Zeeman states of the same fine-structure state should vanish. The atomic states $|1\rangle$, $|2\rangle$, and $|3\rangle$ from Fig. 1 have the same parity and, therefore, the radiative transitions between these states are electric-dipole forbidden. Besides the use of real-valued Rabi frequencies, setting the nondiagonal terms H_{12}, H_{13}, and H_{23} to zero are the only approximations included in our calculations. In the density matrix equation (14), the diagonal terms (for $j = 1, 2,$ and 3) are

$$H_{jj} - H_{00} = \hbar(i\gamma_{j0} + \Delta_j) = \hbar\beta_j, \tag{18}$$

while the rest of the terms are calculated similarly as Eq. (2) from [24]:

$$H_{22} - H_{11} = \hbar[i(\gamma_{20} - \gamma_{10}) + \Delta_1 - \Delta_2] = \hbar\beta_4, \tag{19}$$
$$H_{33} - H_{22} = \hbar[i(\gamma_{30} - \gamma_{20}) + \Delta_2 - \Delta_3] = \hbar\beta_5, \tag{20}$$
$$H_{33} - H_{11} = \hbar[i(\gamma_{30} - \gamma_{10}) + \Delta_1 - \Delta_3] = \hbar\beta_6. \tag{21}$$

Under these conditions, the steady-state solution of the master equation (14) leads to the following atomic coherences

$$\rho_{01} = \frac{\Omega_2\rho_{21} + \Omega_3\rho_{31} - \Omega_1}{2(\Delta_1 + i\gamma_{01})}, \tag{22}$$
$$\rho_{02} = \frac{\Omega_1\rho_{12} + \Omega_3\rho_{32} - \Omega_2}{2(\Delta_2 + i\gamma_{02})}, \tag{23}$$
$$\rho_{03} = \frac{\Omega_1\rho_{13} + \Omega_2\rho_{23} - \Omega_3}{2(\Delta_3 + i\gamma_{03})}, \tag{24}$$
$$\rho_{12} = \frac{\Omega_1\rho_{02} - \Omega_2\rho_{01}}{2(-\Delta_1 + \Delta_2 + i\gamma_{12})}, \tag{25}$$
$$\rho_{13} = \frac{\Omega_1\rho_{03} - \Omega_3\rho_{01}}{2(-\Delta_1 + \Delta_3 + i\gamma_{13})}, \tag{26}$$
$$\rho_{23} = \frac{\Omega_2\rho_{03} - \Omega_3\rho_{02}}{2(-\Delta_2 + \Delta_3 + i\gamma_{23})}. \tag{27}$$

Because the Hamiltonian (17) is Hermitian, the coherences are complex conjugate numbers: $\rho_{ij} = \rho_{ji}^*$. The substitution of Eqs. (25) to (27) into Eqs. (22) to (24) leads to the following coherences:

$$\rho_{01} = \frac{2\Omega_1\beta_4\beta_5}{\alpha_1} + \frac{\Omega_1\Omega_2\beta_5}{\alpha_1}\rho_{02} + \frac{\Omega_1\Omega_3\beta_4}{\alpha_1}\rho_{03}, \tag{28}$$

where

$$\alpha_1 = \left(4\beta_1\beta_4\beta_5 + \Omega_2^2\beta_5 + \Omega_3^2\beta_4\right), \tag{29}$$
$$\rho_{02} = \frac{2\Omega_2\beta_4\beta_6}{\alpha_2} + \frac{\Omega_2\Omega_3\beta_4}{\alpha_2}\rho_{03} - \frac{\Omega_1\Omega_2\beta_6}{\alpha_2}\rho_{01}, \tag{30}$$

where

$$\alpha_2 = \left(4\beta_2\beta_4\beta_6 - \Omega_3^2\beta_4 - \Omega_1^2\beta_6\right), \tag{31}$$
$$\rho_{03} = \frac{2\Omega_3\beta_5\beta_6}{\alpha_3} - \frac{\Omega_1\Omega_3\beta_6}{\alpha_3}\rho_{01} - \frac{\Omega_2\Omega_3\beta_5}{\alpha_3}\rho_{02}, \tag{32}$$

where

$$\alpha_3 = \left(4\beta_3\beta_5\beta_6 - \Omega_1^2\beta_6 - \Omega_2^2\beta_5\right). \tag{33}$$

The coherences ρ_{01}, ρ_{02}, and ρ_{03} can be written in terms of α_j coefficients ($j = 1, \ldots, 11$) as follows:

$$\rho_{01} = \frac{\alpha_8}{\alpha_7} + \frac{\alpha_9}{\alpha_7}\left(\frac{\alpha_{10}}{\alpha_{11}}\right), \tag{34}$$
$$\rho_{02} = \frac{\alpha_{10}}{\alpha_{11}}, \tag{35}$$
$$\rho_{03} = \frac{\alpha_5}{\alpha_4} - \frac{\alpha_6}{\alpha_4}\left(\frac{\alpha_{10}}{\alpha_{11}}\right), \tag{36}$$

where

$$\alpha_4 = \left(\alpha_1\alpha_3 + \Omega_1^2\Omega_3^2\beta_4\beta_6\right), \tag{37}$$
$$\alpha_5 = \left(2\beta_5\beta_6\Omega_3\alpha_1 - 2\Omega_1^2\Omega_3^2\beta_5\beta_6\right), \tag{38}$$
$$\alpha_6 = \left(\Omega_2\Omega_3\Omega_1^2\beta_5\beta_6 + \Omega_2\Omega_3\beta_5\alpha_1\right), \tag{39}$$
$$\alpha_7 = \alpha_4, \tag{40}$$
$$\alpha_8 = \left(2\Omega_1\beta_4\beta_5\alpha_3 + 2\Omega_1^2\Omega_3^2\beta_5\beta_6\right), \tag{41}$$
$$\alpha_9 = \left(\beta_5\Omega_1\Omega_2\alpha_3 - \Omega_3^2\Omega_2\Omega_1\beta_4\beta_5\right), \tag{42}$$
$$\alpha_{10} = (2\beta_4\beta_6\Omega_2\alpha_4 + \beta_4\Omega_2\Omega_3\alpha_5 - \Omega_1\Omega_2\beta_6\alpha_8), \tag{43}$$
$$\alpha_{11} = (\alpha_2\alpha_4 + \beta_4\Omega_2\Omega_3\alpha_6 + \Omega_1\Omega_2\beta_6\alpha_9). \tag{44}$$

Equations (34) and (36) show that ρ_{01} and ρ_{03} depend explicitly on ρ_{02} and will be used to set up EITs in both atomic states $|1\rangle$ and $|3\rangle$ using a common coupling field resonant to the transition $|0\rangle \rightarrow |2\rangle$. The remaining coherences are

$$\rho_{12} = \frac{\Omega_2\alpha_7}{2\beta_4\alpha_4} + \left(\frac{\Omega_2\alpha_8}{2\beta_4\alpha_4} - \frac{\Omega_1}{2\beta_4}\right)\left(\frac{\alpha_{10}}{\alpha_{11}}\right), \tag{45}$$

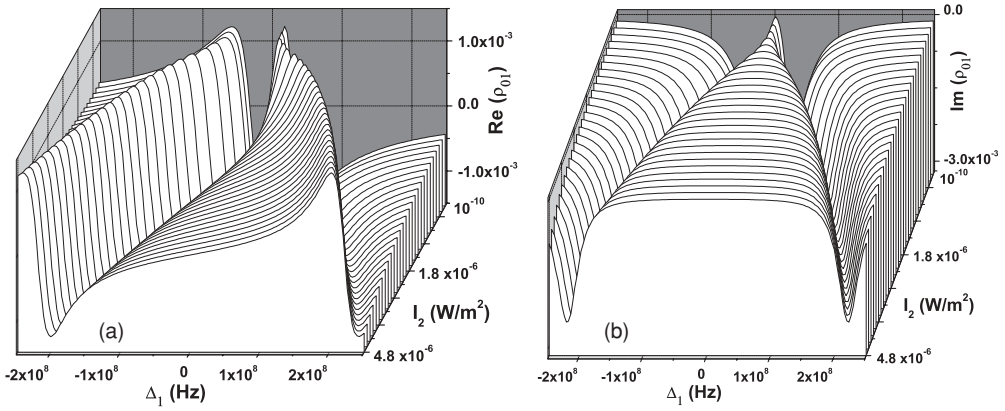

FIG. 2. (a) Real [Re(ρ_{01})] and (b) imaginary [Im(ρ_{01})] parts of the ρ_{01} coherence as a function of probe detuning, Δ_1 for $B = 0.02$ T and I_2 varying from 10^{-10} W/m^2 (the last layer in the back) to 4.8×10^{-6} W/m^2 (first layer in front).

$$\rho_{13} = \frac{\Omega_2\alpha_7}{2\beta_5\alpha_4} - \frac{\Omega_1\alpha_5}{2\beta_5\alpha_4} + \left(\frac{\Omega_2\alpha_8}{2\beta_5\alpha_4} + \frac{\Omega_1\alpha_6}{2\beta_5\alpha_4}\right)\left(\frac{\alpha_{10}}{\alpha_{11}}\right), \quad (46)$$

$$\rho_{23} = \frac{\Omega_2\alpha_5}{2\beta_6\alpha_4} + \left(\frac{\Omega_2\alpha_6}{2\beta_6\alpha_4} + \frac{\Omega_3}{2\beta_6}\right)\left(\frac{\alpha_{10}}{\alpha_{11}}\right), \quad (47)$$

and they are not relevant for our present study.

The next section reports and discusses results for the atomic coherences ρ_{01}, ρ_{03}, and ρ_{02} obtained as steady-state solutions of the master equation (14). These coherences include the essential information regarding the possibility for the formation of EITs inside the absorption bands of the atomic states $|1\rangle$, $|2\rangle$, and $|3\rangle$ from Fig. 1.

IV. FORMATION AND EVOLUTION OF TWO SIMULTANEOUS EITs USING A COMMON COUPLING FIELD

A. Results for ρ_{01} and ρ_{03} coherences

The solutions of the density matrix master equation leads to the ρ_{01} and ρ_{03} coherences reported in Figs. 2 and 3 , respectively. We calculate ρ_{01} from Eq. (34) and ρ_{03} from Eq. (36) as functions of probe detuning varying from -2.5×10^8 to 2.5×10^8 Hz (for best resolution) and at fixed values of intensities. We choose the probe fields $I_1 = 10^{-12}$ W/m^2 and $I_3 = 10^{-7}$ W/m^2 and vary the common coupling field of intensity I_2 from 10^{-10} to 4.8×10^{-6} W/m^2. Our choice of intensities is done so that, in one case, we fulfill the necessary condition for creating an EIT feature at any value of the coupling field (I_2), because the probe field (I_1) is much weaker than the coupling field for any I_2, while for the other probe (I_3) we have two regions: one with the coupling field I_3 stronger than I_2 and another one with $I_2 > I_3$.

The coherences are complex functions,

$$\rho_{01} = \mathrm{Re}(\rho_{01}) + i\mathrm{Im}(\rho_{01}), \quad (48a)$$

$$\rho_{03} = \mathrm{Re}(\rho_{03}) + i\mathrm{Im}(\rho_{03}). \quad (48b)$$

Therefore, in Figs. 2 and 3 we report separately the real [Figs. 2(a) and 3(a)] and imaginary [Figs. 2(b) and 3(b)] parts for 28 layers, which are different by the value of I_2. In our calculations the detuning of the coupling field is set at 3×10^6 Hz and the B field is chosen to be 0.02 T, which is a value in the middle of the range imposed by the boundary conditions (10) and (11). Figures 2 and 3 show

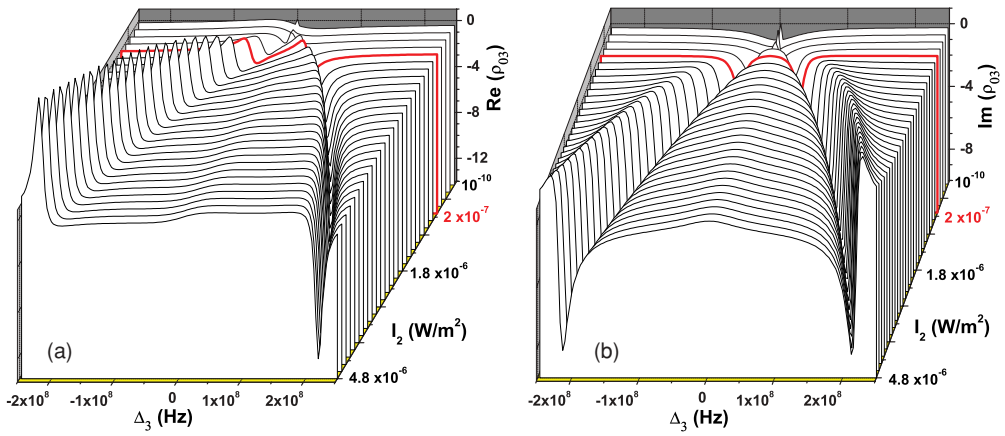

FIG. 3. (Color online) (a) Real [Re(ρ_{03})] and (b) imaginary [Im(ρ_{03})] parts of ρ_{03} coherence as a function of probe detuning Δ_3 for the same B field and the same values of I_2 as in Fig. 2. The thick line (red color in the online version) is the layer 7 (counted from back to front) for a coupling field with $I_2 = 2 \times 10^{-7}$ W/m^2, and indicates from where the probe field is weaker than the coupling field and implicitly the EIT conditions from [9] are fulfilled.

results for coherences calculated with the lowest value for I_2 of 10^{-10} W/m^2, shown as the last layer in the back and with the largest I_2 value of 4.8×10^{-6} W/m^2 shown as the first layer in front. This choice facilitates the comparison between the EIT phases of both coherences, which will be discussed in detail later in Section IV B. The imaginary part of the coherence gives information regarding the mechanism which creates absorption or transparency in the atomic system for a probe E field resonant to an atomic transition, while the real part tells us about the efficiency in slowing down the probe field in the absorption band of an upper state [9]. We notice that the absorption profile for both ρ_{01} and ρ_{03} coherences plotted versus the respective probe detuning looks very similar to the four-level atomic tripod system shown in Fig. 3 from [16].

For the three-level atom V and Λ systems, Fleischhauer *et al.* [9] have established that EIT exists when the following two conditions are fulfilled simultaneously: (1) the Rabi frequency of the coupling field Ω_c should be larger than the radiative decay rate of the $|j\rangle$ state ($\Omega_c > \Gamma_j$) and (2) Ω_c should be larger that the Rabi frequency of the probe field. In our case, the ρ_{01} coherence fulfills these conditions for any values of I_2 because the probe Rabi frequency Ω_1 of 2×10^5 Hz (for $I_1 = 10^{-12}$ W/m^2) is much smaller than both the radiative decay of 7.9×10^7 Hz and Ω_2. For the ρ_{03} coherence shown in Fig. 3, we have $\Omega_3 = 6.3 \times 10^7$ Hz for $I_3 = 10^{-7}$ W/m^2 and, therefore, the EIT phase is established only for $\Omega_2 \geqslant 8.9 \times 10^7$ Hz (or equivalently, for $I_2 \geqslant 2 \times 10^{-7}$ W/m^2).

B. Criteria for formation and evolution of two simultaneous EIT features

For a very weak coupling field, such as $I_3/I_2 \sim 10^3$, an absorption profile is observed in Im(ρ_{03}) coherence of our W scheme (open squares in Fig. 4). As the intensity I_2 increases,

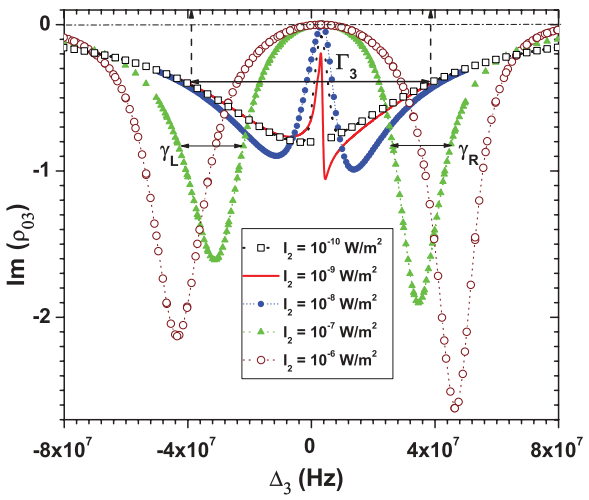

FIG. 4. (Color online) Im(ρ_{03}) versus the probe detuning Δ_3. The formation and evolution of an Autler-Townes doublet in the absorption profile of the Im(ρ_{03}) coherence, for selected intensities I_2 [from Fig. 3(b)] of the coupling field, given in the legend, and for a probe field of $I_3 = 10^{-7}$ W/m^2. The widths γ_R and γ_L measured at FWHM of each resonance of the Autler-Townes doublet are indicated. The width Γ_3 of the atomic state $|3\rangle$ is also indicated between vertical dashed arrows.

a very narrow window with a steep variation and centered on the atomic resonance starts to form in Im(ρ_{03}). In this case, the coupling field acts upon the atomic state $|3\rangle$ as a weak perturbation to a stronger probe field [21] and it produces a very narrow EIT-like feature, which is just a sharp transmission window with a band width smaller than the natural width Γ_3 (of $\sim 7.9 \times 10^7$ Hz) of the state $|3\rangle$ [see the case $I_3/I_2 \sim 10^2$ (full line) in Fig. 4]. This feature gets larger as I_2 increases, as for $I_3/I_2 \sim 10$ (dots) and $I_3/I_2 \sim 1$ (triangles) from Fig. 4.

An EIT phase exists for $I_2 \geqslant 2 \times 10^{-7}$ W/m^2, where a two-photon resonance structure, called an Autler-Townes doublet [25], can be observed in the absorption region of the Im(ρ_{03}) coherence. An EIT feature is defined as being the region between the two-photon resonance of an Autler-Townes doublet [9]. When the coupling field is much stronger than the probe field, the total full width at half maximum (FWHM) of the Autler-Townes doublet, defined as $\gamma = \gamma_L + \gamma_R$ in Fig. 4, becomes constant with the variation of the coupling field. Indeed, as Fig. 4 shows, the FWHM γ varies from 6.2×10^7 Hz (with $\gamma_L = 3.5 \times 10^7$ Hz and $\gamma_R = 2.7 \times 10^7$ Hz) for $I_2 = 10^{-8}$ W/m^2 (dots), to 3.6×10^7 Hz (with $\gamma_L = 1.9 \times 10^7$ Hz and $\gamma_R = 1.7 \times 10^7$ Hz) for $I_2 = 10^{-7}$W/m^2 (triangles), and has a constant value of 3.4×10^7Hz (with $\gamma_L = 1.9 \times 10^7$ Hz and $\gamma_R = 1.5 \times 10^7$ Hz) for $I_2 \geqslant 2 \times 10^{-7}$ W/m^2 (open circles). An EIT phase is characterized by a constant value of the total width γ of the Autler-Townes doublet with the increase in the intensity of the coupling field. Using a different approach, Scully and Zubairy [18] reached the same conclusion for the formation of an "EIT-like" structure, which becomes an EIT feature for a coupling field stronger than the probe.

C. Transit time from a normal dispersive region into an EIT region

The Autler-Townes doublet separates the normal dispersive region from the EIT region: outside the two-photon resonance, the normal dispersive region is driven by the probe field, while the EIT region is driven by the coupling field which completely eliminates the absorption of the probe field, thus creating transparency. In our case, the Zeeman state becomes transparent to the probe field in the region where Im(ρ) ~ 0. The reciprocal of the width (γ) measured at the FWHM of an Autler-Townes doublet represents the transit time from the normal dispersive region into the EIT region. Figure 5 shows EITs for ρ_{01} [Fig. 5(a)] and ρ_{03} [Fig. 5(b)] when a common coupling field I_2 of 4×10^{-7}W/m^2 is used.

The interaction between the E field and a bulk of atoms can be understood using the classical Lorentz model for E-field–electric-dipole interaction [26]. Outside an Autler-Townes doublet, the ensemble of atomic dipoles oscillates with the detuned frequency of the probe field, and therefore intense probe fields should produce larger oscillations. Indeed, in the region of normal dispersion, the Re(ρ_{03}) coherence is larger than the Re(ρ_{01})coherence, as shown in Fig. 5. In the EIT region and for a coupling field much stronger than the probe field (the ρ_{01} coherence case), the transit time between the two regions is shorter, while for a stronger probe field, as for ρ_{03} when $I_2 < 10^{-7}$ W/m^2 [shown in Fig. 3(b)], the transit time between the two regions is longer (or the two-photon resonance is narrower). In the latter case, a "hump" appears

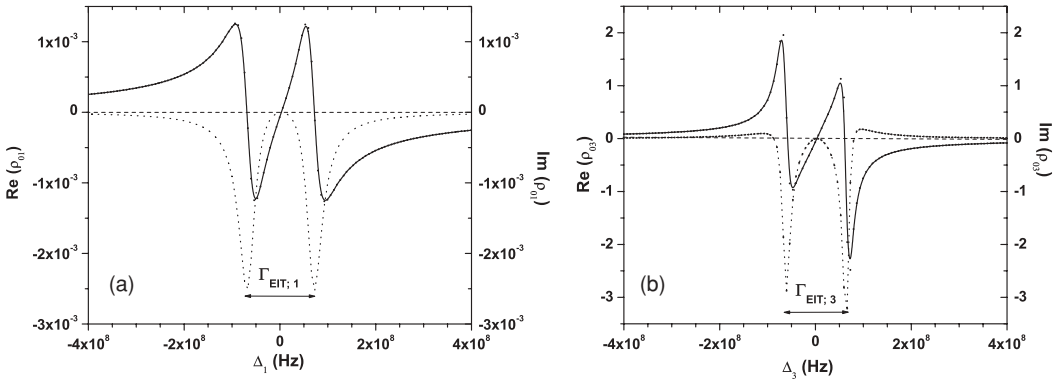

FIG. 5. Two examples of EIT features in the (a) ρ_{01} and (b) ρ_{03} coherences for a coupling field of intensity $I_2 = 4 \times 10^{-7}\,\mathrm{W/m^2}$. The full line represents the real part (left vertical axis) and the dotted line represents the imaginary part (right vertical axis) of the coherences. The width $\Gamma_{\mathrm{EIT};j}$ of each EIT feature in $\mathrm{Im}(\rho_{01})$ $(j = 1)$ and $\mathrm{Im}(\rho_{03})$ $(j = 3)$ is indicated by a double-headed arrow.

on the outside wings of the Autler-Townes doublet, as one can see in Fig. 3(b). This "hump" feature does not appear for $\mathrm{Im}(\rho_{01})$ because the probe field is too weak and the coupling field blocks efficiently the absorption of the probe field near the atomic resonance.

On the other hand, when the probe field is much weaker than the coupling field, like for ρ_{01}, then the sum of the FWHM for the two-photon resonances in the Autler-Townes doublet, $\gamma = \gamma_{\mathrm{L}} + \gamma_{\mathrm{R}}$, equals the natural width Γ_j of the atomic state $|j\rangle$ and the two-photon resonances of the Autler-Townes doublet have the same width and amplitude, as shown in Fig. 6. If the probe field is weaker than the coupling field but is very close in magnitude (see the ρ_{03} case for $I_2 \geqslant 2 \times 10^{-7}\,\mathrm{W/m^2}$), then the Autler-Townes doublet becomes asymmetric, $\gamma_{\mathrm{L}} \neq \gamma_{\mathrm{R}}$ (with $\gamma_{\mathrm{L}} = 1.9 \times 10^7$ Hz and $\gamma_{\mathrm{R}} = 1.5 \times 10^7$ Hz), and the net FWHM of the two-photon resonance γ of 3.4×10^7 Hz is smaller than the width of a Zeeman state, Γ_3 of 7.9×10^7 Hz. The asymmetry can be attributed to a shift of state $|2\rangle$ closer to the dressed state $|3\rangle$, which makes the transit time from the normal dispersive region into the EIT region shorter. Our results are consistent with those obtained by Wielandy and Gaeta [21] for the ladder system.

In conclusion, when a probe field is very weak the transit time from the normal dispersive region to the EIT region is the shortest and equals the lifetime of the atomic state $\gamma = \Gamma_j$, but as the probe field gets stronger, the transit time increases due to a stronger interaction between the atomic dipoles and the probe field near the atomic resonance.

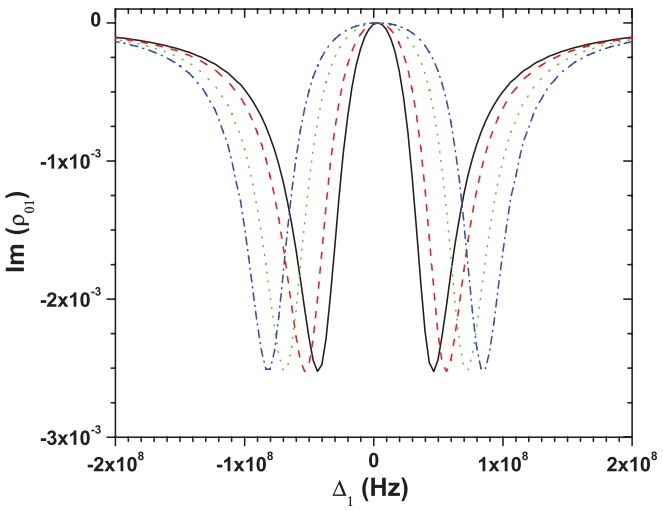

FIG. 6. (Color online) Variation of $\mathrm{Im}(\rho_{01})$ with the probe detuning Δ_1 for several intensities of the coupling field (I_2): $10^{-7}\,\mathrm{W/m^2}$ (full black line), $2 \times 10^{-7}\,\mathrm{W/m^2}$ (dashed red line), $4 \times 10^{-7}\,\mathrm{W/m^2}$ (dotted green line), and $6 \times 10^{-7}\,\mathrm{W/m^2}$ (dot-dashed blue line).

D. Width of EIT region

The width Γ_{EIT} of the EIT feature is the separation distance between the two-photon resonance of an Autler-Townes doublet. An analysis of our data for the case of a probe field much weaker then the coupling field (i.e., ρ_{01} coherence) leads to the well-known formula for the V or Λ systems [9,11]:

$$\Gamma_{\mathrm{EIT}} = \Omega_2. \tag{49}$$

For a nonperturbative probe field (i.e., ρ_{03} coherence), the probe detuning, Δ_p should be also included:

$$\Gamma_{\mathrm{EIT}} = \sqrt{\Omega_2^2 + \Delta_p^2}. \tag{50}$$

Equation (50) is consistent with the result reported by Wielandy and Gaeta [21] for the ladder system (where the width was named the generalized Rabi frequency). In the limit of small probe detuning, Eq. (50) converges to Eq. (49).

The widths of the ρ_{01} and ρ_{03} coherences in the EIT region calculated with Eqs. (49) and (50), increase linearly with the Rabi frequency Ω_2, as shown in Fig. 7. A similar linear variation was observed in the four-level atomic tripod system from [16]. Experiments done with Zeeman sublevels of Rubidium atomic vapors in a three-level atomic system proved that indeed the width of an EIT region increases with the intensity of the coupling field when the probe field is kept constant [27]. In our W system, for a strong coupling field ($I_2 \geqslant 2 \times 10^{-6}\,\mathrm{W/m^2}$), the widths of both coherences converge (within 1% difference) toward a common value of 2.8×10^8 Hz. In this case, the system behaves like two independent V systems driven by a strong coupling field (I_2).

According to Ye and Zibrov [28], studies of the width of EIT feature may lead to a better understanding of various processes which can influence the atomic coherences, such as collisional

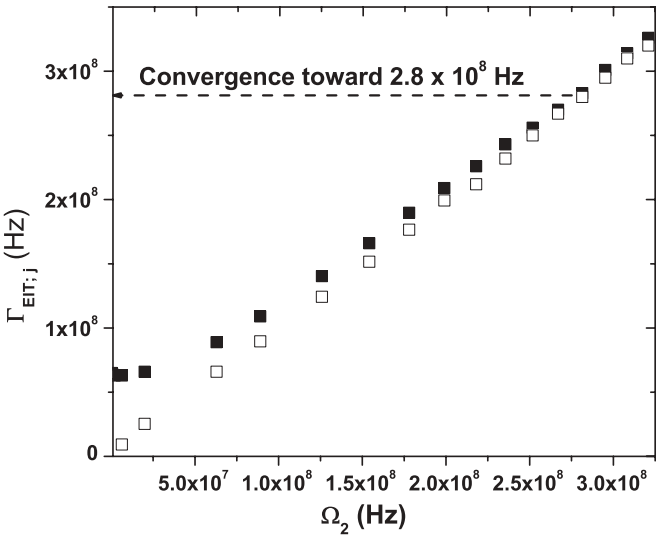

FIG. 7. Variation of the EIT widths of ρ_{01} (full squares, $j = 1$) and ρ_{03} (open squares, $j = 3$) coherences with Rabi frequency Ω_2 associated to an adjustable coupling field.

relaxations, spontaneous transfer of coherence, and Doppler broadening. Therefore, our present results could be used as reference for future studies which will include decoherence effects.

E. Influence of coupling field's detuning on position of Autler-Townes doublet

Figure 8 shows the shift in the position of the two resonances of the Autler-Townes doublet in the ρ_{01} coherence for a few values of the coupling detuning. Although no change in $\Gamma_{\rm EIT}$ was observed for any change in the value of the coupling detuning, the location of $\mathrm{Im}(\rho_{01}) = 0$ does change. The $\mathrm{Im}(\rho_{01})$ coherence is indeed close to zero in the region near the zero detuning of the probe field, but it is exactly zero at $\Delta_p = \Delta_c$, which indicates that the middle of an Autler-Townes doublet is driven by the coupling field. When the detuning Δ_c changes by $\tilde{\Delta}$, the EIT feature shifts by the same $\tilde{\Delta}$. Figure 8 shows an increase of Δ_c from 3×10^6 to 9×10^6 Hz. This change shifts the EIT feature to the right by 6×10^6 Hz.

F. Variation of slope for Re(ρ) with the coupling field

For an atomic system in an EIT phase, the group velocity of the probe field varies inverse proportionally with the slope of $\mathrm{Re}(\rho)$ measured with respect to the probe detuning (Δ_p) [13]. In a narrow interval of Δ_p where $\mathrm{Im}(\rho) \sim 0$ [see Figs. 2(b) and 3(b)], $\mathrm{Re}(\rho)$ from Figs. 2(a) and 3(a) varies linearly with Δ_p. Figure 9 shows the variation of the slopes $d\mathrm{Re}(\rho_{0j})/d\Delta_j$ near $\mathrm{Im}(\rho_{0j}) \sim 0$ with Ω_2 of the coupling field, for both ρ_{0j}, where $j = 1$ or 3. We observe that, in the EIT phase, the slope of $\mathrm{Re}(\rho)$ decreases rapidly as the intensity of the coupling field increases, reaching a threshold value when the net coupling field is much stronger than the probe field. The slope of $\mathrm{Re}(\rho_{01})$ decreases rapidly with Ω_2, starting from very low values for I_2, while for $\mathrm{Re}(\rho_{03})$, the slope first increases sharply at low values of the coupling field, reaching a maximum at $I_2 = 8 \times 10^{-9}$ W/m^2, and decreases fast, reaching a threshold

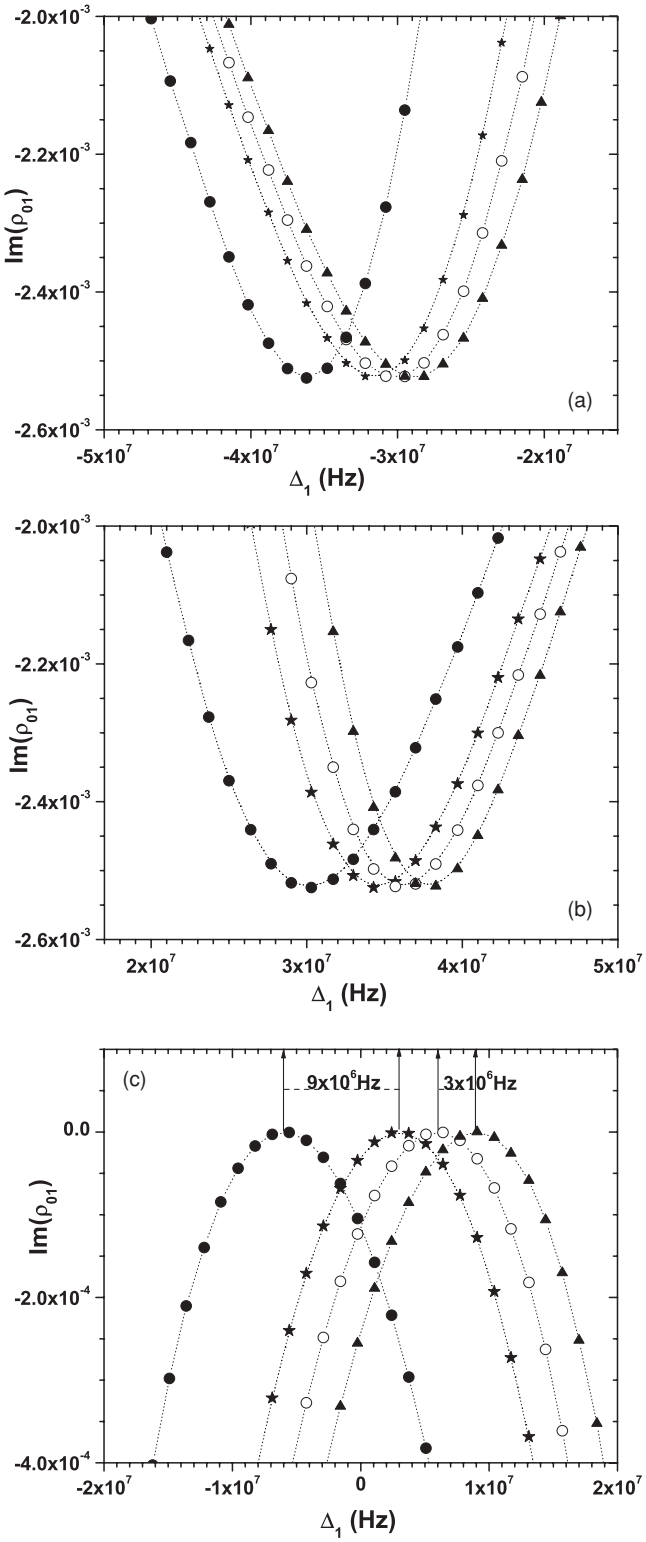

FIG. 8. Shift of $\mathrm{Im}(\rho_{01})$ with the coupling detuning for $\Delta_2 = \Delta_3 = 3 \times 10^6$ Hz (stars), 6×10^6 Hz (circles), 9×10^6 Hz (triangles), and -6×10^6 Hz (dots). Here, we use $I_2 = 10^{-8}$ W/m^2. Case (a) shows the (virtual) photon located at the left-hand side of the Autler-Townes doublet, (b) shows the (virtual) photon located at the right-hand side, while (c) is the central part of the EIT region near the zero probe detuning. The shift between adjacent cases is shown in the central part of $\mathrm{Im}(\rho_{01})$ (e.g., calculations done with $\Delta_2 = \Delta_3 = 3 \times 10^6$ Hz and -6×10^6 Hz give a shift of 9×10^6 Hz).

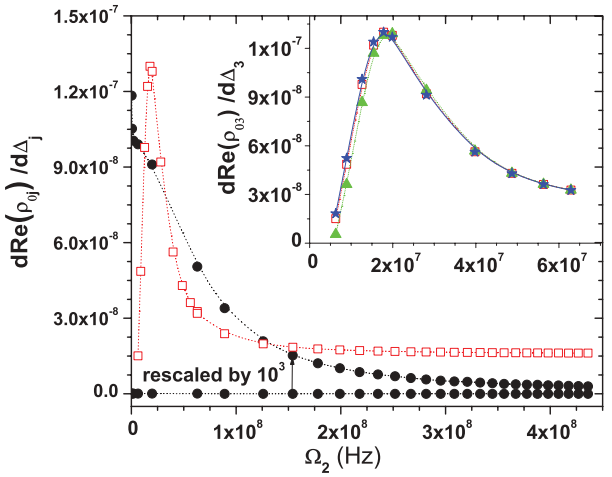

FIG. 9. (Color online) Variation of $d\mathrm{Re}(\rho_{01})/d\Delta_1$ (dots) and $d\mathrm{Re}(\rho_{03})/d\Delta_3$ (open squares) with the Rabi frequency Ω_2 of the coupling field. In order to compare the slopes, we rescale $d\mathrm{Re}(\rho_{01})/d\Delta_1$ by 10^3. The inset shows the variation of the slope $d\mathrm{Re}(\rho_{03})/d\Delta_3$ for small values of Ω_2 and for B fields of 0.01 T (triangles), 0.02 T (open squares), and 0.03 T (stars).

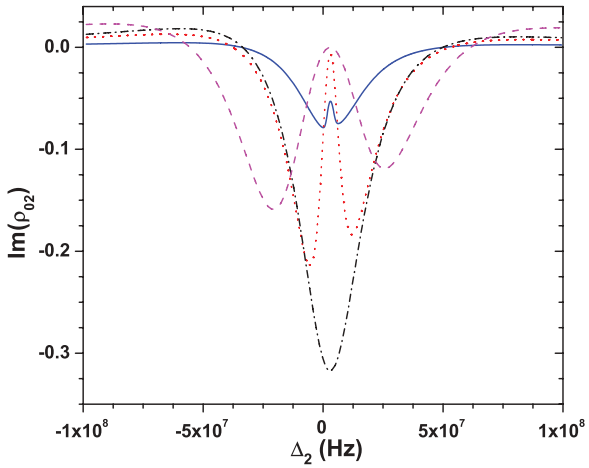

FIG. 10. (Color online) $\mathrm{Im}(\rho_{02})$ coherence versus the probe detuning Δ_2 for a few selected probe intensities I_2: 10^{-9} W/m^2 (full blue line), 10^{-8} W/m^2 (dotted red line), 10^{-7} W/m^2 (dashed magenta line), and 6×10^{-7} W/m^2 (dot-dashed black line).

value for $I_2 \geqslant 2 \times 10^{-6}$ W/m^2. The difference in magnitude between the slopes for $\mathrm{Re}(\rho_{01})$ and $\mathrm{Re}(\rho_{03})$ [$d\mathrm{Re}(\rho_{03})/d\Delta_3$ is about 10^3 times larger than $d\mathrm{Re}(\rho_{01})/d\Delta_1$] is due to the difference between the intensities of the probe fields. The slope for $\mathrm{Re}(\rho_{03})$ has a steeper variation than for $\mathrm{Re}(\rho_{01})$ because the probe field is stronger in the former than the latter case. Our calculations suggest that a stronger probe field can be slowed down more efficiently than a weaker probe.

Another interesting aspect is the invariance of the EIT feature to the change of the B field. The inset to Fig. 9 shows that, once the system is inside an EIT phase, whether the B field is weaker (0.01 T) or stronger (0.03 T) than the reference value of 0.02 T used in our calculations reported in Figs. 2 and 3, the change in the slope of $\mathrm{Re}(\rho)$ is negligible. Thus, for $I_2 < I_3$ only a small change of a few percent can be observed in the slope of $\mathrm{Re}(\rho_{03})$. In conclusion, we have observed that when the B field takes on values in the range established by the boundary conditions (10) and (11), there is no significant change in the transit time from the normal dispersive region to EIT region (see Section IV C), or in the width Γ_{EIT} from Section IV D.

G. Evolution of ρ_{02} coherence when ρ_{01} and ρ_{03} are in an EIT phase

Figure 10 shows the imaginary part of the ρ_{02} coherence calculated from Eq. (35). We see that $\mathrm{Im}(\rho_{02})$ develops a narrow EIT-like feature due to the coupling field $I_1 + I_3 \cong I_3$ (since $I_3 \gg I_1$) inside the absorption region of the transition $|0\rangle \rightarrow |2\rangle$ at low probe fields, I_2. When I_2 reaches a value of 2×10^{-7}W/m^2, making $I_2 > I_3$, the state $|2\rangle$ becomes opaque. The variation of $\mathrm{Im}(\rho_{02})$ agrees with the interpretation based on atomic oscillations induced by the strongest E field from Sec IV C. Our results from Fig. 10 indicate that a four-level atomic W system cannot have three simultaneous EITs.

H. Influence of pressure broadening on characteristics of EIT features

The inclusion of the collisional dephasing in the master equation (13) will be reported in a future work because of the elaborate calculations involved. However, we can report here the influence of the atomic collisions on the EIT feature though the inclusion of the pressure broadening on the Zeeman levels. It is known that collisions enlarge the width of the atomic states, thus decreasing their lifetime [19] according to the uncertainty principle. It is interesting to see the variation of the slope of the coherences, as well as the width of the EIT features with increasing the width of the excited Zeeman state $|j\rangle$.

Figures 11 and 12 show the evolution of real and imaginary parts of the ρ_{0j} coherences when the width Γ_j of the atomic state $|j\rangle$ increases by a factor N, the B field is 0.02 T, and for a combination of intensities ($I_1 = 10^{-12}$ W/m^2, $I_2 = 10^{-6}$ W/m^2, and $I_1 = 10^{-7}$ W/m^2) which allows us to have EIT for both ρ_{01} and ρ_{03}. We show 30 layers defined by values of N varying from 1 to 15 and take an even increment of 0.5 added to the width Γ_j used for the previous layer as we linearly increase Γ_j from one layer to the next. We see that a linear increase of Γ_j changes both the slope $d\mathrm{Re}(\rho_{0j})/d\Delta_j$ and the width Γ_{EIT}. Figure 13 shows the exponential decrease of the slopes for the ρ_{01} and ρ_{03} coherences, with a steeper variation for slow collisions and shallower variation for fast collisions. Therefore, the group velocity of the probe field increases with the increase of the frequency between atomic collisions.

The variation of Γ_{EIT} for ρ_{01} and ρ_{03} from Fig. 14 shows that for very weak probe fields (such as in the ρ_{01} case) the width Γ_{EIT} increases linearly with a linear increase of the atomic width (and so does the transit time from the normal dispersive region to the EIT region), while for a stronger probe field (such as for the ρ_{03} case) the width Γ_{EIT} increases logarithmically for slow atomic collisions and slightly linear for faster collisions. When the atomic widths of the transparent states $|0\rangle$ and $|3\rangle$ are both exactly 4 times the natural width Γ_j of the respective state

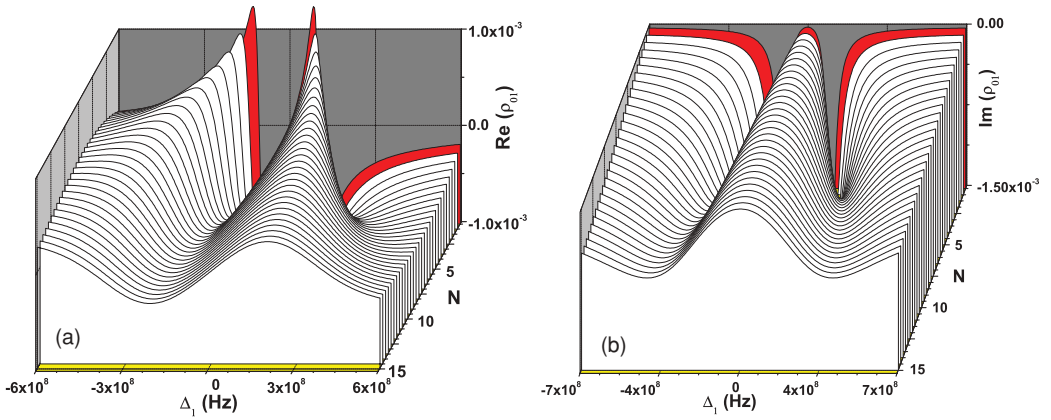

FIG. 11. (Color online) (a) Real [Re(ρ_{01})] and (b) imaginary [Im(ρ_{01})] parts of ρ_{01} coherence plotted as a function of the probe detuning Δ_1 for several widths Γ_1 increasing by a factor N. We choose the probe intensity $I_1 = 10^{-12}\,\mathrm{W/m^2}$ and the coupling intensity $I_2 = 10^{-6}\,\mathrm{W/m^2}$, while I_3 is $10^{-7}\,\mathrm{W/m^2}$. The B field is 0.02 T. We show 30 layers using values of N from 1 (the last red layer in the back) to 15 (the first layer in front) with an even increment of 0.5, as we go from one layer to the next.

(which is for $N = 4$) we get the same value of Γ_{EIT} for both the ρ_{01} and ρ_{03} coherences ($\Gamma_{\mathrm{EIT};1} = \Gamma_{\mathrm{EIT};3}$). Larger increments of Γ_j increases Γ_{EIT} faster for ρ_{01} than for ρ_{03}. This means that an increase in the frequency of collisions allows a weaker probe field to form a wider EIT region than a stronger probe for the same coupling field.

V. ANALYSIS OF EIT REGION USING A DRESSED-STATE REPRESENTATION

The evolution of ρ_{01} and ρ_{03} coherences can be understood in several equivalent ways. One way considers the EIT features as the result of destructive interference between two (virtual) photons of the Autler-Townes doublet (see Fig. 4) [9]. Another way is by analyzing the eigenvalues of the atom-field interaction Hamiltonian from (6) [9,18]. Our preliminary studies revealed the complexity of interpreting EIT structures using these eigenvalues and, therefore, we plan to present such an analysis elsewhere.

A third way is by adopting the picture of destructive interference between the direct pathway created by one (circularly polarized) probe field and the combination of indirect pathways induced by the other two fields (the other circularly polarized field and the linearly polarized field). For ρ_{01} and ρ_{03} coherences, the direct pathway corresponds to the atomic transitions $|0\rangle \to |1\rangle$ or $|0\rangle \to |3\rangle$, respectively, reported in Section IV. In this approach, the direct pathway $|0\rangle \to |1\rangle$ of the σ^- polarized probe field interferes destructively with the pathways $|0\rangle \to |3\rangle \to |1\rangle$, $|0\rangle \to |2\rangle \to |1\rangle$, and $|0\rangle \to |3\rangle \to |2\rangle \to |1\rangle$. Similarly, the direct pathway $|0\rangle \to |3\rangle$ of the σ^+ polarized field interferes destructively with $|0\rangle \to |1\rangle \to |3\rangle$, $|0\rangle \to |2\rangle \to |3\rangle$, and $|0\rangle \to |1\rangle \to |2\rangle \to |3\rangle$. The many indirect pathways that need to be considered make such an analysis very difficult. Because our master equation (13) does not include the collisional dephasing due to the intramultiplet transitions between Zeeman states of the $|^1P_1\rangle$ state, a model based explicitly on the interference between pathways is not actually adequate for interpreting the EIT features from Figs. 2 and 3. Instead, we shall look for a meaningful way to interpret these two EITs.

Our approach is based on the fact that the density matrix master equation (13) is basis-set independent as long as the

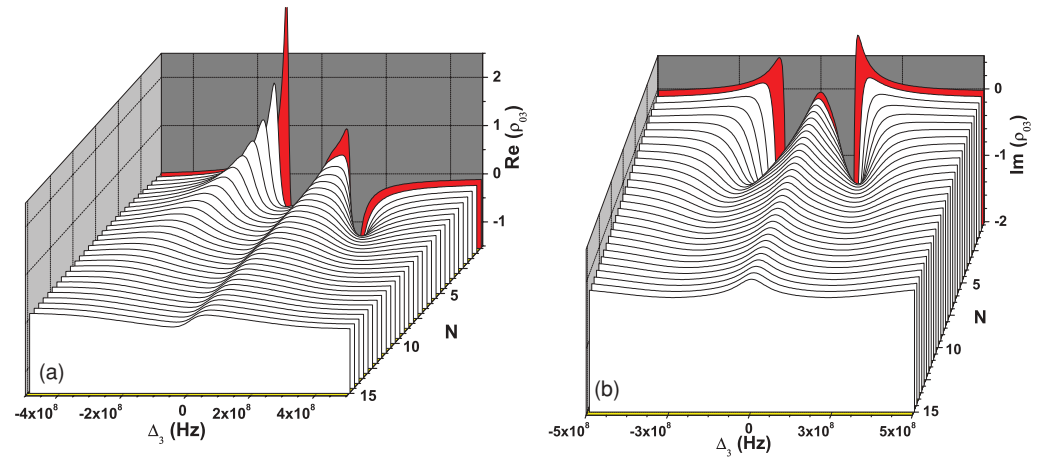

FIG. 12. (Color online) (a) Similar to Fig. 11, but for ρ_{03} coherence as a function of probe detuning Δ_3. We use the same intensities ($I_1 = 10^{-12}\,\mathrm{W/m^2}$, $I_2 = 10^{-6}\,\mathrm{W/m^2}$, $I_3 = 10^{-7}\,\mathrm{W/m^2}$) and B field value of 0.02 T as in Fig. 11.

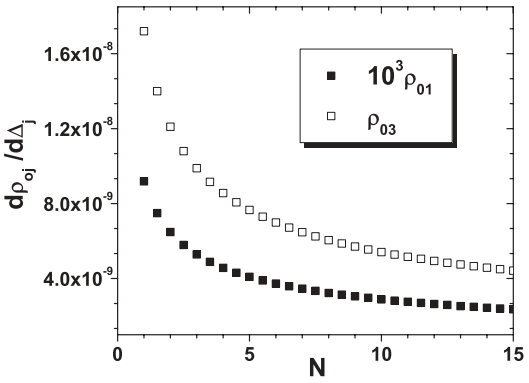

FIG. 13. Variation of the slopes of ρ_{01} (full squares) and ρ_{03}(open squares) coherences for values of N varying from 1 to 15 with an increment of 0.5, selected from Figs. 11 and 12, respectively. The results for the ρ_{01} coherence are rescaled by 10^3 to compare with the ρ_{03} case.

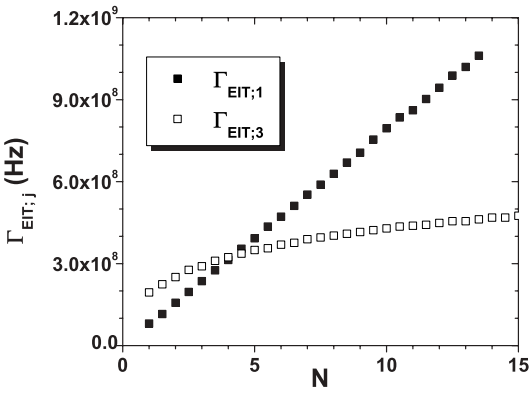

FIG. 14. Variation of width $\Gamma_{\mathrm{EIT};j}$ of ρ_{01} (full squares, $j = 1$) and ρ_{03}(open squares, $j = 3$) for values of N from 1 to 15 with an increment of 0.5, selected from Figs. 11 and 12, respectively.

chosen basis is complete and orthogonal. Therefore, we prefer to adopt a dressed-state representation with three coupling states $|C_1\rangle$, $|C_2\rangle$, and $|C_3\rangle$ and one noncoupling state $|\mathrm{NC}\rangle$. These four dressed states should form an orthogonal basis set constructed as linear superposition of atomic "bare" states $\{|0\rangle,|1\rangle,|2\rangle,|3\rangle\}$ and should include the couplings between the probe and coupling fields with the atomic dipole moments.

According to [9], the state $|\mathrm{NC}\rangle$ of the atom-field interaction Hamiltonian, H from Eq. (17) should have zero eigenvalue. Also, $|\mathrm{NC}\rangle$ should be orthogonal on the population trapped ground state $|0\rangle$ [18]. We choose to define the noncoupling dressed state as

$$|\mathrm{NC}\rangle = \frac{\Omega_2\Omega_3|1\rangle - 2\Omega_1\Omega_3|2\rangle + \Omega_1\Omega_2|3\rangle}{\Omega_D}, \qquad (51)$$

where $\Omega_D = (\Omega_1^2\,\Omega_2^2 + 4\,\Omega_1^2\,\Omega_3^2 + \Omega_2^2\,\Omega_3^2)^{1/2}$ represents a normalization constant. One can easily check that the requirements: $H|\mathrm{NC}\rangle = 0$ [9] and $\langle 0\,|\mathrm{NC}\rangle = 0$ [18] are simultaneously verified. The state $|\mathrm{NC}\rangle$ is built upon the idea that a noncoupling state should not include the atomic ground state $|0\rangle$, but should include the interaction between the other three excited atomic states $|j\rangle$ (with $j = 1$, 2, or 3) with the two fields nonresonant to the atomic transition $|0\rangle \rightarrow |j\rangle$. For example, in the state $|\mathrm{NC}\rangle$, the bare atomic state $|1\rangle$ interacts only with the coupling fields "2" and "3", etc. Such a criterion implicitly accounts for the quantum interference between various pathways in the W-type system. The state $|\mathrm{NC}\rangle$ includes explicitly the coupling terms responsible for the creation of an EIT feature. Our procedure of building the state $|\mathrm{NC}\rangle$ was inspired in part from an article by Gu *et al.* [15] regarding a five-level M-type atom.

The orthogonal coupling states $|C_j\rangle$ are built so that each E_j field couples with a linear combination of the dressed atomic states. Each state $|C_j\rangle$ includes an interaction term between the excited state $|j\rangle$ and the ground state $|0\rangle$ (through a coefficient κ_j), as well as the term $\Omega_j\tilde{\Omega}$ which represents the field-atomic states interaction mixing:

$$|C_j\rangle = \frac{\kappa_j|0\rangle + \Omega_j\tilde{\Omega}}{\Omega_D}, \qquad (52)$$

where $\tilde{\Omega}$ is a linear combination of dressed atomic states: $\Omega_1|1\rangle + \Omega_2|2\rangle + \Omega_3|3\rangle$. The conditions

$$\langle \mathrm{NC}|C_j\rangle = 0 \quad \text{and} \quad \langle C_i|C_j\rangle = 0\,(\text{when } i \neq j) \qquad (53)$$

are verified if both dressed states $|\mathrm{NC}\rangle$ and $|C_j\rangle$ include the same constant Ω_D.

Our new orthogonal basis set allows us to understand the mechanism responsible for the formation simultaneously of two EIT's in our W scheme using a one-to-one correlation between bare atomic states $|j\rangle$ and coupling states $|C_j\rangle$. For example, the atomic state $|1\rangle$ is associated with the dressed state $|C_1\rangle$ because it allows a stronger interaction with the (probe) field E_1 (resonant to the transition $|0\rangle \rightarrow |1\rangle$) than any other state through the term $\Omega_1\tilde{\Omega}$. Similarly, the dressed states $|C_2\rangle$ and $|C_3\rangle$ are correlated to the atomic states $|2\rangle$ and $|3\rangle$, respectively.

We will interpret the formation of EITs in our W system by projecting the dressed states $|\mathrm{NC}\rangle$ and $|C_j\rangle$ on the atomic states. Thus, the coupling between a Zeeman state $|j\rangle$ and $|\mathrm{NC}\rangle$ is given by

$$\gamma_j^2 = \langle j \mid NC\rangle^2 \propto \left(\frac{\Omega_i\Omega_k}{\Omega_D}\right)^2, \qquad (54)$$

where i and $k \neq j$, while the coupling between the ground state $|0\rangle$ and the state $|C_j\rangle$ is given by

$$\kappa_j^2 = \langle 0|C_j\rangle^2 = \frac{\Omega_j^2\sum_{l=1}^{3}\Omega_l^2}{\Omega_D^2}, \qquad (55)$$

and indicates the absorption of the E_j field by state $|j\rangle$. The interpretation of the coefficients defined in Eqs. (54) and (55) is that an atomic state $|j\rangle$ becomes transparent to a probe field when it strongly couples with the dressed state $|\mathrm{NC}\rangle$ and γ_j^2 is large. If the ground state $|0\rangle$ couples with a dressed state $|C_j\rangle$, then the coefficient κ_j^2 is large and the atomic state $|j\rangle$ is opaque to (or absorbs) the E_j field.

The coefficients γ_j^2 and κ_j^2 are not probability amplitudes, because our coupling states $|C_j\rangle$ are not normalized to 1. However, they provide a clear physical meaningful interpretation for the evolution of the ρ_{01} (from Fig. 2), ρ_{03} (from Fig. 3) and ρ_{02} (from Fig. 10) coherences in our W system consistent with our quantum results. It is worthwhile to note that, for each $|j\rangle$ state, the coefficients κ_j^2 and γ_j^2 have opposite

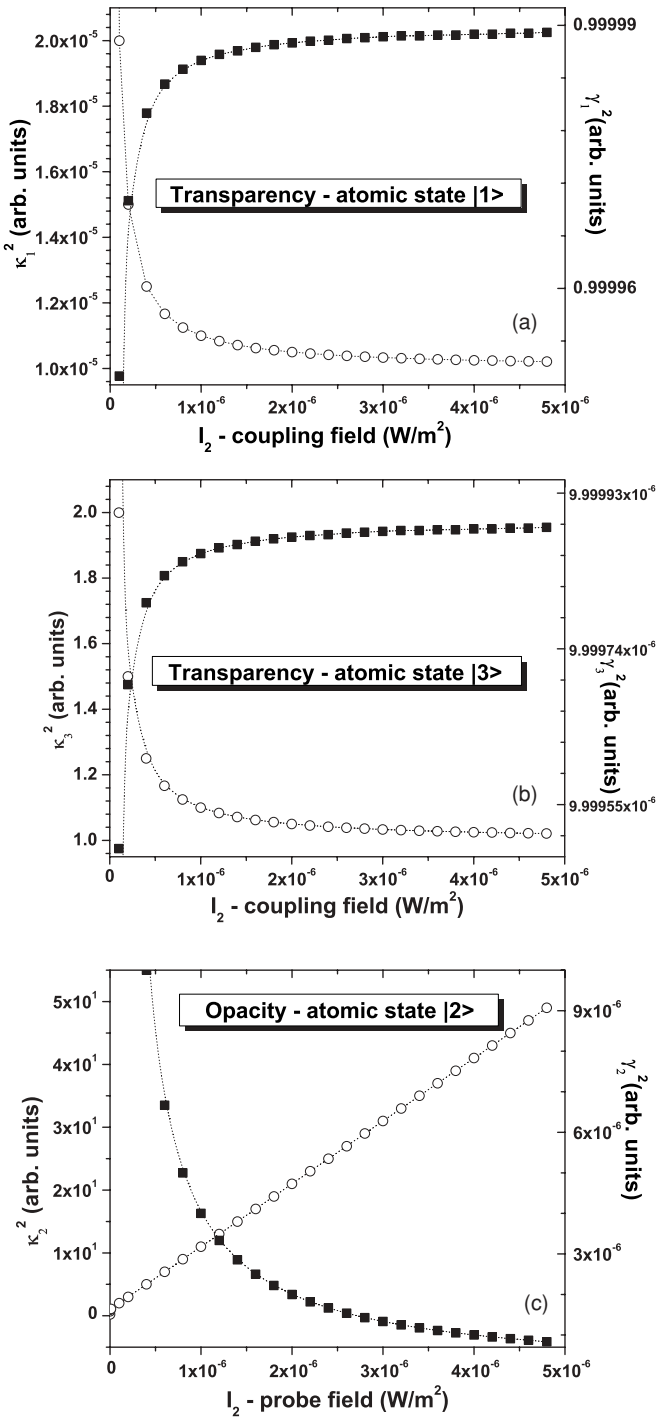

FIG. 15. The variation of coefficients $\gamma_j^2 = \langle j \,|\mathrm{NC}\rangle^2$ (full squares) and $\kappa_j^2 = \langle 0 \,|\, C_j\rangle^2$(open circles), where $j = 1$, 2, or 3, as defined in Eqs. (54) and (55) respectively, for (a) ρ_{01}, (b) ρ_{03}, (c) and ρ_{02}.

variations. This property is consistent with the transparency or opacity of a certain atomic state $|j\rangle$ to a probe field. For example, the variation of coefficients κ_1^2 and γ_1^2 from Fig. 15(a) explains well the formation and the evolution of an EIT feature in state $|1\rangle$, and it is consistent with the variation of our quantum coherence ρ_{01} reported in Fig. 2. Similarly, the coupling coefficient κ_3^2 has a variation with I_2 opposite to γ_3^2, as shown in Fig. 15(b). This is consistent with our results for ρ_{03} from Fig. 3.

Our basis set $\{|\mathrm{NC}\rangle, |C_1\rangle, |C_2\rangle, |C_3\rangle\}$ provides a qualitative explanation for the formation and the evolution of two simultaneous EITs in two atomic states, while the third state typically shows opacity [see Fig. 15(c)]. The rate of variation of the coefficients γ_j^2 and κ_j^2 with an increase in the intensity of the coupling field(s) is consistent with the evolution of an EIT phase, as discussed in Section IV B; thus, when the coupling field is not very strong, the coefficients γ_j^2 have a sharp increase with the increase of I_2. Once the system is inside the EIT phase, the coefficients γ_j^2 have a much shallower variation with the increase of I_2 [see Figs. 15(a) and 15(b)]. The opacity of state $|2\rangle$ [Fig. 15(c)] is indicated by an increase of the interaction coefficient κ_2^2 with the increase in intensity I_2 of (now) the probe field. We believe that our present method could be generalized to any other multi-level, multi-laser system.

VI. CONCLUSION

This article provides a detailed presentation of the formation and evolution of two simultaneous EIT features in a four-level atomic W system interacting simultaneously with three optical fields. Also, it presents the necessary criteria for establishing EIT in a W scheme. Our results suggest that a W scheme could be eventually used in storage of optical information in dense atomic media using binary recording with two (opposite) circularly polarized photonic beams driven by a linearly polarized coupling field. Our W scheme could be considered as the reverse of a tripod system, such as the one reported in [14], but here we predict two simultaneous EITs for two distinctive probe fields induced by a stronger coupling field, while Paspalakis and Knight [14] proposed a setting which allowed slowing down a single probe field with two different group velocities by using simultaneously two coupling fields with different detunings.

We have observed that, when the coupling field is only a perturbation to a strong probe field, a narrow transmission window forms and gradually enlarges with the increase in intensity of the coupling field. When the coupling field is stronger than the probe field, the EIT phase can be reached and an Autler-Townes doublet forms with a constant width γ measured at FWHM, while the group velocity becomes stationary with an increase in strength of the coupling field. A qualitative analysis for the formation of EIT features in our four-level atomic W system can be done using an intuitive dressed-state representation, including a descriptive account of the interaction between three E fields and four atomic levels. We simulate the collisional relaxation by including the pressure broadening of the excited Zeeman states and we observe when the width of these states increases linearly, the slope of the atomic coherences decreases exponentially and the width Γ_{EIT} of the Autler-Townes doublet increases linearly for a very weak probe, while for a stronger probe field, Γ_{EIT} shows a slower logarithmic increase. We believe that the methods proposed in this article can be applied to more sophisticated systems.

ACKNOWLEDGMENTS

We wish to thank the anonymous referee for his valuable comments.

[1] A. Imamoglu and S. E. Harris, Opt. Lett. **14**, 1344 (1989); K. J. Boller, A. Imamoglu, and S. E. Harris, Phys. Rev. Lett. **66**, 2593 (1991); J. E. Field, K. H. Hahn, and S. E. Harris, *ibid.* **67**, 3062 (1991).

[2] M. Fleischhauer and M. D. Lukin, Phys. Rev. Lett. **84**, 5094 (2000); M. M. Kash *et al.*, *ibid.* **82**, 5229 (1999).

[3] L. V. Hau, S. E. Harris, Z. Dutton, and C. H. Behroozi, Nature (London) **397**, 594 (1999).

[4] C. Liu, Z. Dutton, C. H. Behroozi, and L. V. Hau, Nature (London) **409**, 490 (2001); A. Kasapi, M. Jain, G. Y. Yin, and S. E. Harris, Phys. Rev. Lett. **74**, 2447 (1995); D. F. Phillips, A. Fleischhauer, A. Mair, R. L. Walsworth, and M. D. Lukin, *ibid.* **86**, 783 (2001).

[5] S. E. Harris, Phys. Rev. Lett. **62**, 1033 (1989); M. O. Scully, S.-Y. Zhu, and A. Gavrielides, *ibid.* **62**, 2813 (1989); A. Imamoglu, J. E. Field, and S. E. Harris, *ibid.* **66**, 1154 (1991); M. O. Scully and M. Fleischhauer, Science **263**, 337 (1994).

[6] H. Sun, Y. Niu, S. Jin, and S. Gong, J. Phys. B.: At. Mol. Opt. Phys. **40**, 3037 (2007); M. Paternostro, M. S. Kim, and B. S. Ham, Phys. Rev. A **67**, 023811 (2003).

[7] B. K. Dutta and P. K. Mahapatra, Phys. Scr. **75**, 345 (2007).

[8] F. Li, H. Xiong, and M. S. Zubairy, Phys. Rev A **72**, 010303 (2005).

[9] M. Fleischhauer, A. Imamoglu, and J. P. Marangos, Rev. Mod. Phys. **77**, 633 (2005).

[10] L. Zhou and H. Xiong, J. Phys. B.: At. Mol. Opt. Phys. **41**, 025501 (2008); P. Zhou and S. Swain, Phys. Rev. Lett. **78**, 832 (1997).

[11] C. W. Neff, L. M. Andersson, and M. Qiu, New J. Phys. **9**, 48 (2007).

[12] R.-Y. Chang, W.-C. Fang, Z.-S. He, B.-C. Ke, P.-N. Chen, and C.-C. Tsai, Phys. Rev. A **76**, 053420 (2007); B. K. Dutta and P. K. Mahapatra, J. Phys. B.: At. Mol. Opt. Phys. **39**, 1145 (2006).

[13] M. Mahmoudi, R. Fleischhaker, M. Sahrai, and J. Evers, J. Phys. B.: At. Mol. Opt. Phys. **41**, 025504 (2008).

[14] E. Paspalakis and P. L. Knight, J. Opt. B: Quantum Semiclass. Opt. **4**, S372 (2002).

[15] Y. Gu, L. Wang, K. Wang, C. Yang, and Q. Gong, J. Phys. B.: At. Mol. Opt. Phys. **39**, 463 (2006).

[16] L. Yang, L. Zhang, X. Li, L. Han, G. Fu, N. B. Manson, D. Suter, and C. Wei, Phys. Rev. A **72**, 053801 (2005).

[17] Y. Gu, Q. Sun, and Q. Gong, Phys. Rev. A **67**, 063809 (2003).

[18] M. O. Scully and M. S. Zubairy, *Quantum Optics*, 5th ed. (Cambridge University Press, 2006).

[19] B. H. Bransden and C. J. Joachain, *Physics of Atoms and Molecules* (Longman Scientific & Technical, NY, 1994).

[20] I. I. Sobelman, *Atomic Spectra and Radiative Transitions*, 2nd ed. (Springer-Verlag, Berlin, 1992), Chap. 9.

[21] S. Wielandy and A. L. Gaeta, Phys. Rev. A **58**, 2500 (1998).

[22] L. Windholz, Phys. Scr. T **95**, 81 (2001).

[23] M. Fleischhauer and A. S. Manka, Phys. Rev. A **54**, 794 (1996).

[24] J. Gea-Banacloche, Y. Li, S. Jin, and M. Xiao, Phys. Rev. A **51**, 576 (1995).

[25] S. H. Autler and C. H. Townes, Phys. Rev. **100**, 703 (1955).

[26] E. Hecht, *Optics*, 4th ed. (Addison Wesley, San Francisco, 2002).

[27] X. Feng, G. Rui-Min, C. Shuai, Z. Yu, L. Lu-Ming, and C. Xu-Zong, Chin. Phys. Lett. **20**, 1257 (2003).

[28] C. Y. Ye and A. S. Zibrov, Phys. Rev. A **65**, 023806 (2002).